ACS APPLIED MATERIALS & INTERFACES

Research Article

www.acsami.org

Grain-Size-Tuned Highly H_2-Selective Chemiresistive Sensors Based on ZnO–SnO_2 Composite Nanofibers

Akash Katoch,[†] Zain Ul Abideen,[†] Hyoun Woo Kim,*[,‡] and Sang Sub Kim*[,†]

[†]Department of Materials Science and Engineering, Inha University, Incheon 402-751, Republic of Korea

[‡]Division of Materials Science and Engineering, Hanyang University, Seoul 133-791, Republic of Korea

Supporting Information

ABSTRACT: We investigated the effect of grain size on the H_2-sensing behavior of SnO_2-ZnO composite nanofibers. The $0.9SnO_2$-$0.1ZnO$ composite nanofibers were calcined at 700 °C for various times to control the size of nanograins. A bifunctional sensing mechanism, which is related not only to the SnO_2-SnO_2 nanograins, but also to the ZnO-SnO_2 nanograins with surface metallization effect, is responsible for the grain-oriented H_2-sensing properties and the selective improvement in sensing behavior to H_2 gas compared to other gases. Smaller grains are much more favorable for superior H_2 sensing in SnO_2-ZnO composite nanofibers, which will be an important guideline for their use in H_2 sensors. The one-dimensional nanofiber-based structures in the present study will be efficient in maximizing the sensing capabilities by providing a larger amount of junctions.

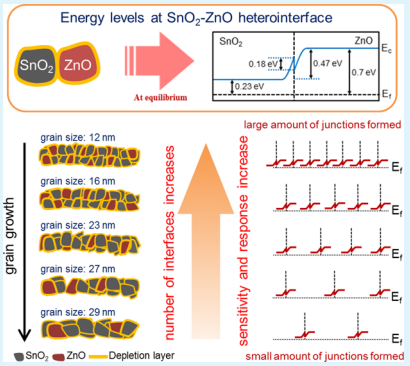

KEYWORDS: *oxide, nanofibers, SnO_2, ZnO, hydrogen, sensors*

1. INTRODUCTION

Hydrogen has recently been regarded as one of the most promising energy sources, considering the air pollution, global warming, and exhaustion of the Earth's energy resources. In particular, hydrogen has several advantages as an energy source; it does not generate the pollution byproducts during its usage as a fuel; it can be easily delivered and stored in a variety of forms; it can be manufactured from water and can be recycled into water; it can be used in various areas, including industrial materials, fuels, automobile, aircraft, fuel cells, etc.

Although hydrogen has a low minimum ignition energy (0.017 mJ)[1] and a high diffusion coefficient (0.61 cm^2/s in air),[2] which is explosive and flammable when the concentration becomes higher than 4% in air,[3] it is colorless, odorless, and tasteless, and is not detectable by human senses.[4] In the current and future industries based on hydrogen economy, the development of the techniques for early and accurate sensing of escaped or leaked hydrogen gas is very important, in order to face safety challenges involving during production, conveyance, and storage of hydrogen gas. Because fast detection of hydrogen gas at its very low concentration is important, there have been numerous reports on the sensing behavior to hydrogen gas. To achieve the high gas detection performance in sensors, considerable efforts have been made to develop the structure/architecture, incorporate new materials, and modify the sensor surface.[5−7]

Very recently, the present group developed a hydrogen sensor with an exceptionally high sensitivity, which is comprised of ZnO nanofibers.[8] Their high sensitivity is partly ascribed to the peculiar structure of nanofibers, providing large grain boundaries. However, the main reason for the sensor enhancement is related to the phenomenon, in which zinc oxide (ZnO) generates metallic surface transitions in the presence of H_2.[9] According to the literature, H_2 tends to act as a shallow donor in ZnO, which contributes to an enhanced conductivity.[10] In the previous work, we proposed the bifunctional mechanisms, in which the regular reducing gas effect that occurs at grain boundaries, not only in SnO_2-SnO_2 homointerfaces, but also in SnO_2-ZnO heterointerfaces. Particularly, in SnO_2-ZnO heterointerfaces, H_2-induced metallization in grain boundaries will enhance the H_2-sensing capabilities.[8]

Because the nanofibers are comprised of a large number of nanograins, the control of the grain size greatly affects various properties, including optical and chemical properties. Accordingly, in the H_2-sensing mechanism with respect to ZnO nanofibers, the control of the grain size greatly affects the sensing behavior. Therefore, in order to fully exploit the H_2-induced metallization in grain boundaries for maximizing the sensing abilities, the systematic investigation on the effect of grains is urgently required. This will provide a guideline for the synthesis of ZnO nanofibers for the future preparation of high-sensitivity hydrogen sensors.

In the present study, we prepared SnO_2-ZnO composite sensors using one-dimensional nanofibers consisting of SnO_2 and ZnO nanograins. Herein, we prepared the SnO_2-ZnO

Received: September 8, 2015
Accepted: January 12, 2016
Published: January 12, 2016

DOI: 10.1021/acsami.5b08416
ACS Appl. Mater. Interfaces 2016, 8, 2486−2494

composite nanofibers with the fixed ratio of SnO_2 and ZnO grains, while systematically changing the grain size by the variation of the calcination time. In other words, we investigated the H_2-sensing capability of SnO_2-ZnO composite nanofibers by controlling the number of heterojunctions between the SnO_2 and ZnO nanograins. In particular, we expect that adsorbed hydrogen will result in a metallic volume on the boundaries of ZnO nanograins, bringing about a drastic enhancement in the selective sensing behavior toward H_2 gas.

2. EXPERIMENTAL SECTION

SnO_2-ZnO composite nanofibers were synthesized using an electrospinning method, where the composition of the electrospinning solution was maintained at xZnO-$(1-x)$$SnO_2$, ($x$ = 0.1). Tin(II) chloride dihydrate ($SnCl_2{\cdot}2H_2O$, Sigma-Aldrich Corp.) and zinc acetate ($Zn(OAc)_2$, Sigma-Aldrich Corp.) were used as precursor materials. The synthesis of SnO_2-ZnO composite nanofibers was carried out as follows. First, we prepared a mixed solvent solution by mixing ethanol (anhydrous, 99.5%, Sigma-Aldrich Corp.) and dimethylformamide (DMF, anhydrous, 99.8%, Sigma-Aldrich Corp.) at a 1:1 ratio. Subsequently, 1.7 g of $SnCl_2{\cdot}2H_2O$ and 0.15 g of $Zn(OAc)_2$ were dissolved in the mixed solvent. After stirring for 1 h, 8 wt % of polyvinylpyrrolidone (PVP, M_w = 1 300 000, Sigma-Aldrich Corp.) was added to the prepared solution, which was then stirred for 10 h to allow complete mixing of the precursor materials. The as-prepared viscous solution was loaded into a syringe with a 21-gauge stainless steel needle with an inner diameter of 0.51 mm. Our previous experiments indicated that as-spun fibers with a smaller outer diameter could be obtained using a needle with a smaller inner diameter.[11,12] The distance between the tip of the needle and the collector, the feed rate of the solution, and the applied voltage were 20 cm, 0.05 mL/h, and 15 kV, respectively, when the collector was grounded. All of the experiments were conducted at room temperature in ambient air. After 15 min of electrospinning, as-spun fibers were found to be uniformly distributed over the SiO_2-grown Si wafers, which were placed on the collector. The thickness of the SiO_2 layer was about 250 nm.

In previous literature, the calcination of SnO_2-ZnO composite nanofibers was intensively studied. For pure ZnO nanofibers, from the TGA data, it was revealed that a calcination temperature of >420 °C was needed to remove the solvent and polymer as well as to fully decompose the zinc acetate into a pure ZnO phase. However, the higher temperature of 600 °C was required to obtain the highly crystalline ZnO structures.[13] For SnO_2-ZnO composite nanofibers of (x)ZnO-$(1-x)$$SnO_2$ ($x \geq 0.45$),[14] there was no change in weight loss above 575 °C, revealing that a calcination temperature of >575 °C is needed to remove the solvent and polymer as well as to fully decompose zinc acetate and tin chloride into a pure ZnO−SnO_2 phase. For SnO_2-ZnO composite nanofibers of xZnO-$(1-x)$$SnO_2$ (x = 0.01−0.50),[15] highly crystalline SnO_2 and ZnO phases in composite nanofibers were obtained through calcination at 700 °C. Furthermore, at this same temperature, complete removal of PVP and PVA polymer was observed. Accordingly, in the present work, the prepared as-spun fibers were then calcined at 700 °C in air for different lengths of time ranging from 0.5 to 24 h. The heating rate was set at 5 °C/min. For both ZnO and SnO_2 nanofibers,[13,16] when the optimal calcination temperature was determined, in which solvent and polymer were completely removed and the high-enough crystallinity was obtained, the decrease in the calcination time decreased the grain size.

The microstructure and phase were analyzed by X-ray diffraction (XRD, Philips X'pert MRD diffractometer), scanning electron microscopy (SEM, Hitachi S-4200), and transmission electron microscopy (TEM, Philips CM-200) with an energy-dispersive X-ray spectrometer (EDX).

Using an interdigital electrode mask, double-layer electrodes of Ti (thickness ∼50 nm) and Au (thickness ∼200 nm) were sequentially deposited via sputtering onto the SnO_2-ZnO composite nanofibers. The sensing ability of the SnO_2-ZnO composite nanofiber sensors to H_2 was investigated in the H_2 concentration range of 0.1 to 10 ppm. All of the sensing measurements were performed at an operating temperature of 350 °C. According to the previous paper, we investigated the dynamic resistance curves and sensor responses of the 0.90SnO_2-0.10ZnO nanofiber to H_2 gas at different temperatures,[15] revealing that the sensor response at 350 °C is lower and higher than 300 and 250 °C, respectively. In Table S1, we show response times/recovery times of the 0.90SnO_2-0.10ZnO nanofiber sensors at H_2 concentrations in the range of 0.1−10 ppm, at temperatures of 250, 300, and 350 °C, respectively. It is noteworthy that both response times and recovery times decrease with increasing the temperature in the range of 250−350 °C. Accordingly, the sensor exhibited the shortest response time/recovery time at 350 °C. The operating temperature of present sensor was set to 350 °C; the shortest response time/recovery time can be obtained, whereas the sensitivity is higher than that of 250 °C.

The gas concentration was controlled by mass flow controllers in order to maintain a balanced mixing ratio of highly purified H_2 (>99.999%) and N_2 gas. The flow rate was set at 500 sccm in the experiments. This experimental configuration is very similar to previously reported setups.[17−20] The sensing abilities of the SnO_2-ZnO composite nanofiber sensors were also tested for other reducing and oxidizing gases including CO, benzene, toluene, ethanol, NO_2, SO_2, H_2S, CO_2. The sensing capabilities of the fabricated sensors were evaluated in terms of their responses in the presence and absence of H_2 gas, defined as R_a/R_g, where R_a is the initial resistance in the absence of H_2 gas, and R_g is the resistance measured in the presence of H_2 gas. To investigate the effect of humidity in sensing test, we compared the sensing behaviors of the 0.90SnO_2-0.10ZnO nanofibers in dry and humid air (RH 30%). In addition, to study the stability in humid environment, we maintained the sensors in the humid environment (RH 60% @ 25 °C) for 6 months and compared the sensing behaviors of the preserved sample with the original one.

3. RESULTS AND DISCUSSION

Figure 1a−e shows SEM images of the SnO_2-ZnO composite nanofibers that were calcined for 0.5, 2, 6, 18, and 24 h, respectively. The SEM images show that all of the composite nanofibers consisted of nanograins, regardless of the calcination time. The insets show corresponding low-magnification SEM images, exhibiting the dense formation of nanofibers with a straight-line morphology. Figure 1f shows the grain size as a function of calcination time, indicating that the grains size increased with increasing calcination time, whereas the diameter of the nanofibers remained constant around ∼90 nm.

Figure 2a is a TEM image of a SnO_2-ZnO composite nanofiber, illustrating the numerous grains present on the nanofiber. The average diameter of the grains is about 12 nm, coinciding with the grain size estimated in Figure 1f. Figure 2b shows the associated selected area electron diffraction (SAED) pattern. The SAED pattern exhibits the diffraction rings, corresponding not only to the (110), (101), (200), and (211) planes of the tetragonal rutile SnO_2 structure (JCPDS: 88−0287), but also to the (101) and (102) planes of the hexagonal ZnO structure (JCPDS: 89−0511). Figure 2c shows the enlarged TEM image of the surface region of the composite nanofiber. Figure 2d shows a lattice-resolved high-magnification TEM image of the enlarged surface region of the squared area in Figure 2c. We estimated that the distances between the lattice fringes are about 0.264 and 0.334 nm, matching d_{101} and d_{110} values of a tetragonal rutile SnO_2 phase, respectively. In addition, the interplanar spacing of approximately 0.247 nm corresponds to the (101) plane of hexagonal ZnO. In previous studies, various nanofibers such as ZnO,[8] CuO,[21] and SnO_2[11] were efficiently fabricated through an electrospinning method, and their sensing properties were significantly altered by varying the grain size. Figure 2e shows a corresponding EDX

DOI: 10.1021/acsami.5b08416
ACS Appl. Mater. Interfaces 2016, 8, 2486−2494

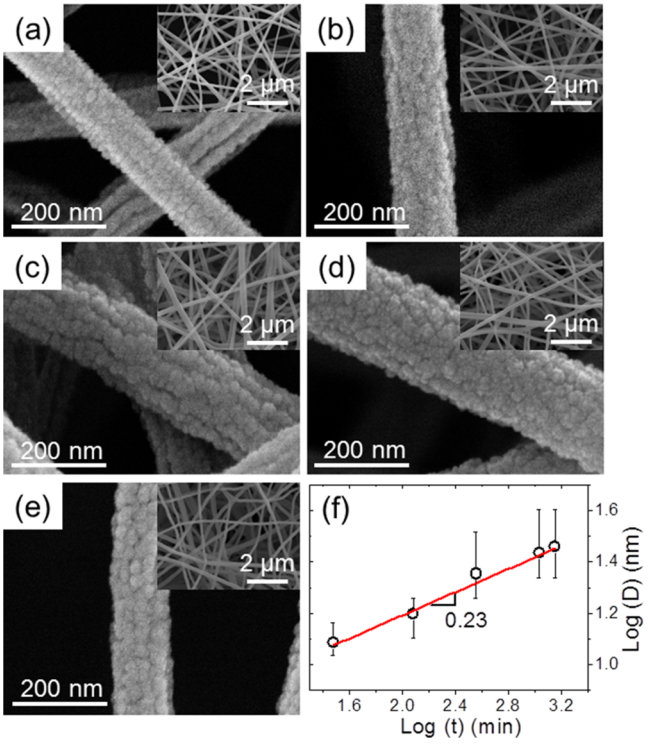

Figure 1. SEM images of SnO_2-ZnO composite nanofibers calcined at 700 °C for different time interval (a) 0.5, (b) 2, (c) 6, (d) 18, and (e) 24 h. (f) Grain size as a function of calcination time in the range of 0.5−24 h.

spectrum, which confirms the presence of Sn, Zn, and O elements. The source of the Cu and C elements is believed to be the carbon-coated Cu grid used in the preparation of the TEM samples. The elemental maps for Sn, Zn and O are plotted in Figure S2.

Figure 3 shows the XRD patterns of the SnO_2-ZnO composite nanofibers with different grain sizes. All recognizable diffraction peaks were related to a hexagonal ZnO structure (JCPDS: 89−0511) or a tetragonal rutile SnO_2 structure (JCPDS: 88−0287). Accordingly, we realize that the calcined composite nanofibers have tetragonal rutile SnO_2 and hexagonal ZnO phases. It is noteworthy that the ZnO peaks are enhanced as the calcination time increases, due to the improved crystalline quality of the nanocrystals. The sizes of crystallites estimated by the XRD main peaks, in conjunction with the Scherrer equation, did not significantly change with changing the calcination time (Text S1). We surmise that the crystallites were agglomerated to form the grains. The SEM-measured grain size, comprising many crystallites, will increase with increasing calcination temperature. Furthermore, it is expected that the boundaries between the crystallites cannot be clearly observed in the SEM images.

To investigate the sensing behavior of the SnO_2-ZnO composite nanofibers to H_2 gas, we measured the dynamic responses while varying the H_2 concentration from 0.1 to 10 ppm (Figure 4). Herein, the response curves were plotted for each composite nanofiber sensor with different grain sizes in the range of 12−29 nm. The resistance decreased with introduction of H_2 and was restored to the initial value upon the removal of H_2 gas. Considering that H_2 is a reducing gas, the composite nanofiber sensors clearly exhibit n-type semiconductor behavior.

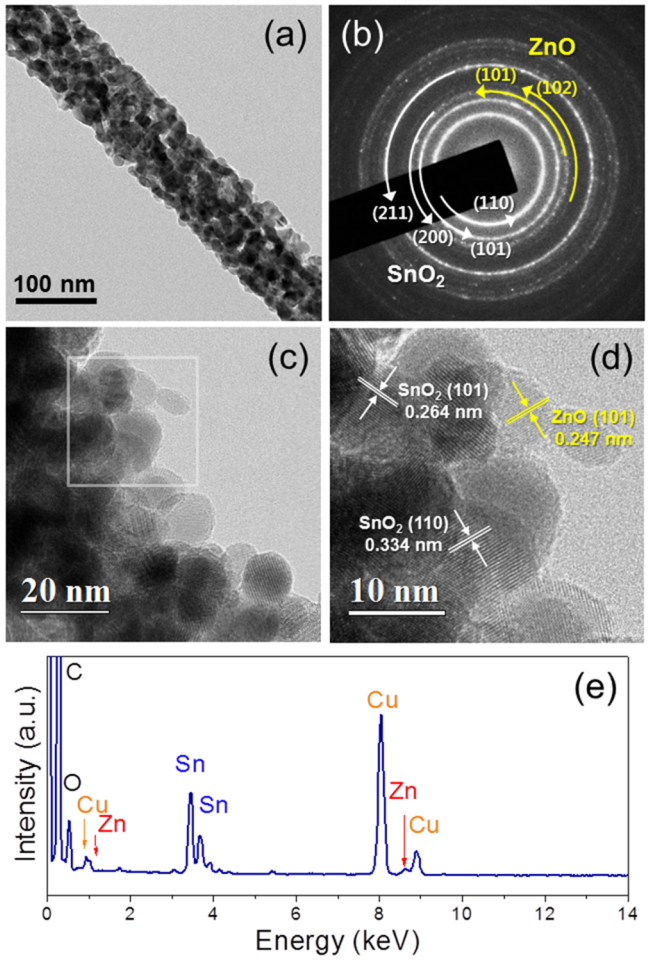

Figure 2. (a) Low-magnification TEM image of a SnO_2-ZnO composite nanofiber. (b) Associated SAED pattern. (c) Enlarged TEM image. (d) Lattice-resolved TEM image of the surface region, enlarging the squared area in c. (e) EDX pattern exhibiting the existence of Sn, Zn, and O elements. The Cu and C signals originate from the carbon-coated Cu TEM grid.

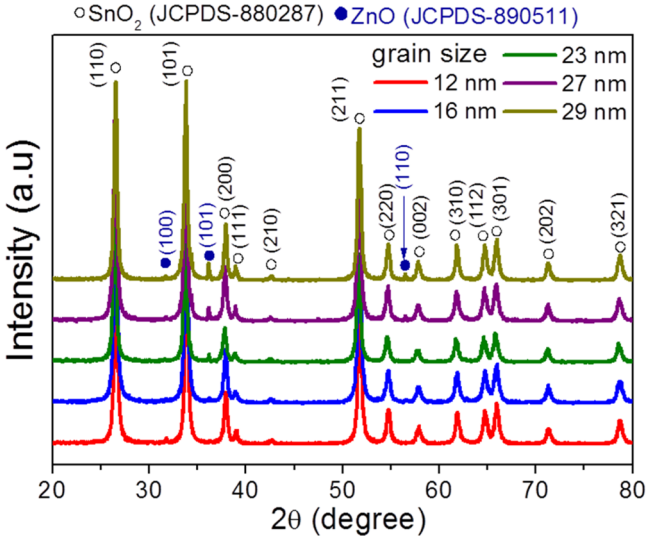

Figure 3. XRD spectra of composite nanofibers with grain size of 12, 16, 23, 27, and 29 nm.

DOI: 10.1021/acsami.5b08416
ACS Appl. Mater. Interfaces 2016, 8, 2486−2494

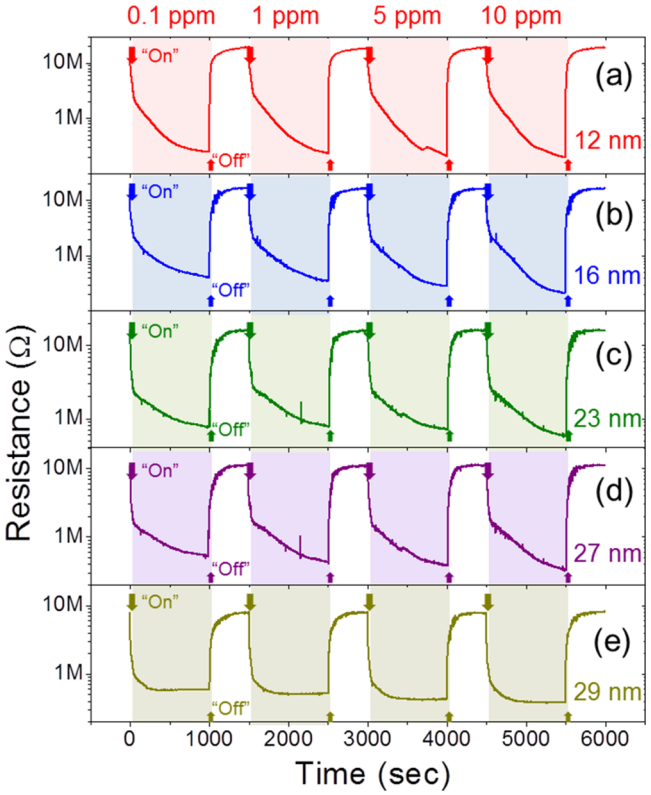

Figure 4. Dynamic resistance curves of the sensors fabricated with SnO_2-ZnO composite nanofibers with grain size of (a) 12, (b) 16, (c) 23, (d) 27, and (e) 29 nm.

Based on Figure 4, the sensor responses of the various composite nanofiber sensors are summarized in Figure 5. As is

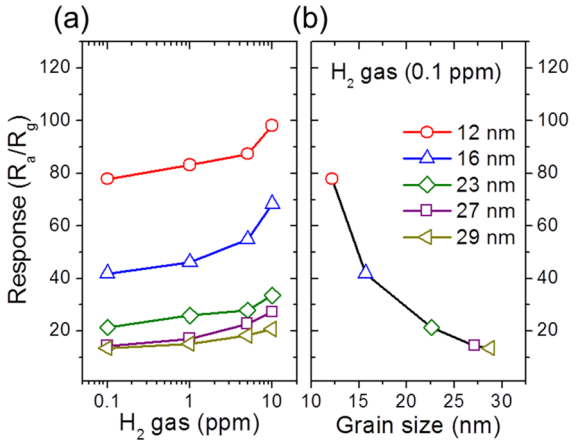

Figure 5. Responses of sensors fabricated with SnO_2-ZnO composite nanofibers with different grain sizes (a) to various H_2 concentrations and (b) 0.1 ppm of H_2.

evident in Figure 5a, the sensor response increased with decreasing grain size for all H_2 gas concentrations in the range of 0.1−10 ppm. The strongest response was observed for the SnO_2-ZnO composite nanofiber sensor with the smallest grain size of 12 nm. In order to evaluate the sensing capability of the composite nanofiber sensors at a very low H_2 concentration, we performed the sensing test at a concentration of 0.1 ppm. Figure 5b summarizes the response as a function of grain size for a fixed H_2 concentration of 0.1 ppm. The sensor responses of the sensors with grain sizes of 12, 16, 23, 27, and 29 nm are 78, 42, 21, 15, and 14, respectively. It is apparent that the response increases as the calcination process becomes shorter. Accordingly, at a low concentration of 0.1 ppm, the smaller grain size results in a stronger sensor response. In order to investigate the detection limit of the SnO_2-ZnO composite nanofiber sensor with the smallest grain size of 12 nm, we carried out the H_2 sensing tests at concentration below 0.1 ppm. At the H_2 concentration of 0.01 ppm, the value of the resistance was not dropped upon the introduction of H_2 gas, revealing that the nanofiber sensor did not operate properly. On the other hand, at the H_2 concentration of 0.03 ppm, the resistance was decreased upon the introduction of H_2 gas (Figure 6). In addition, the resistance was increased and restored to the original value by the removal of the H_2 gas. The sensor response was calculated to be about 3.6.

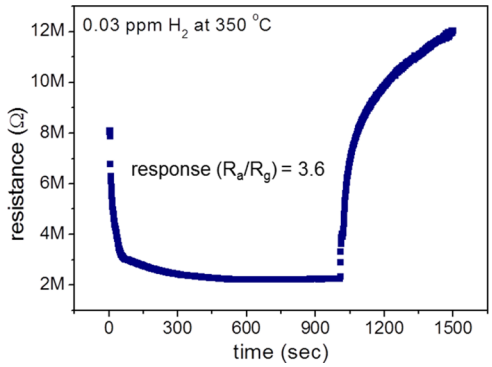

Figure 6. Dynamic resistance curves of sensors fabricated with SnO_2-ZnO composite nanofibers with the grain size of 12 nm to 0.03 ppm of H_2.

We hypothesized a bifunctional mechanism to explain the sensing behavior of SnO_2-ZnO composite nanofibers with respect to H_2 gas; two main mechanisms operate simultaneously in the presence of H_2. First, the homojunctions formed between the SnO_2-SnO_2 nanograin boundaries contribute through the well-known H_2 reducing gas effect. Being similar to SnO_2 nanofibers, homojunctions between two SnO_2 grains are formed. In an air environment, oxygen species such as O_2^-, O^{2-}, and O^- diffuse through the grain boundaries and cover the nanograins.[22,23] Because the absorbed oxygen molecules extract electrons from the conduction band of SnO_2 ($O^{2-}(ads) + e^- \rightarrow 2O^-(ads)$), band bending occurs at the grain boundaries. The potential barrier between adjacent grain boundaries restricts the flow of electrons. These H_2 molecules react with adsorbed oxygen molecules ($H_2 + O^-(ads) \rightarrow H_2O + e^-$), releasing electrons back to SnO_2.[23] In this way, resistance modulation occurs in the SnO_2 nanofibers.

On the other hand, in SnO_2-ZnO composite nanofibers, heterojunctions are generated at the boundaries between SnO_2 and ZnO nanograins. The molar ratio of SnO_2-ZnO composite nanofibers to SnO_2-SnO_2 is 9:1, indicating that only a few SnO_2-ZnO heterojunctions exist in the presence of many SnO_2-SnO_2 homojunctions. Not only SnO_2-SnO_2 homojunctions but also SnO_2-ZnO heterojunctions simultaneously contribute to the reducing gas effect in oxide materials.

Figure 7 displays the sensing mechanism of the composite nanofiber sensors with SnO_2 and ZnO nanograins. It is known that the work functions of n-SnO_2 and n-ZnO are 4.55 and 5.20 eV, respectively. Initially, when SnO_2 and ZnO nanograins

DOI: 10.1021/acsami.5b08416
ACS Appl. Mater. Interfaces 2016, 8, 2486−2494

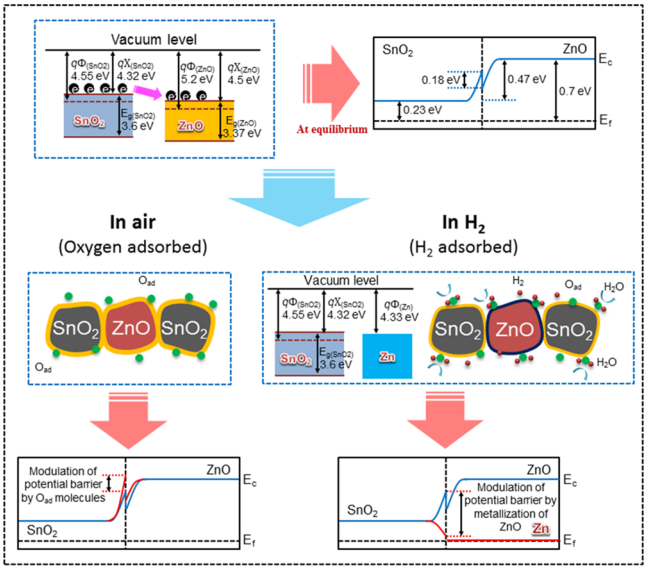

Figure 7. Schematic illustration of the sensing mechanism of the composite nanofiber sensors with ZnO and SnO_2 nanograins.

come into contact, electrons will flow from n-SnO_2 to n-ZnO, due to the difference in work function, until equilibrium in terms of Fermi levels is reached.[24] Initially, at the SnO_2-ZnO heterointerface, an electron accumulation region and an electron depletion region are formed on the ZnO and SnO_2 sides, respectively, ultimately bending the energy band and vacuum energy level. Because the amount of ZnO nanograin is much smaller than that of SnO_2 grain, we expect that the current in the sensor devices will mainly flow through the SnO_2 grains.

Prior to the introduction of H_2 gas, oxygen species diffuse through and cover the SnO_2/ZnO heterojunctions. In ambient air, oxygen is preferentially adsorbed at the grain boundaries of SnO_2 and ZnO, by which the conducting electrons are trapped, and the nanofibers become less conductive.[25] Accordingly, it is suggested that the conduction band near the boundaries will bend upward, increasing the energy difference between the Fermi level and conduction band. The SnO_2 near the grain boundaries becomes more electron-depleted (Figure 7).

To demonstrate the second mechanism, Figure 7 shows the metallization effect between the SnO_2 and ZnO nanograins. With the introduction of reductive H_2 gas, however, the concentration of oxygen species decreases at the nanofiber surface and grain boundaries. Although some active hydrogen species react with the surface oxygen and generate gaseous H_2O, the surface of the ZnO nanograins is metallized.[9,26,27] The adsorption of hydrogen molecules on the nonpolar surfaces of ZnO is responsible for the increased conductivity by metallization of Zn surface atoms.[9,26] The metallization of ZnO has previously been investigated in both experimental and theoretical studies.[9,26] Recently, X-ray photoelectric spectroscopic studies were performed to investigate the surface states of ZnO nanofibers before and after exposure to H_2 gas.[8] The spin orbit splitting for Zn $2p^{3/2}$ and Zn $2p^{1/2}$ was 23.0 and 23.1 eV, which are characteristic of Zn^{2+} and Zn^0 oxidation states in ZnO, respectively.[28−31] The sharing of electrons between the *s*-orbital of H and p-orbital of O through strong hybridization results in delocalization of charge between Zn and O−H. This delocalization of electrons metallizes the surface Zn atoms and is induced by hydrogen.[10]

By the introduction of the H_2 gas molecules, the H_2 gas will reduce the surface adsorbed oxygen species (represented by O_{ad} in Figure 7), however, it is expected that not all adsorbed oxygen will be consumed. If there is no metallization effect, the only effect of H_2 gas will be to reduce the adsorbed oxygen species and thus the variation of the potential barrier by the introduction of H_2 gas will be less than the amount of the change of potential barrier by the adsorption of oxygen. The electrons will be generated by the surface reaction and flow to the SnO_2/ZnO heterointerfaces, decreasing the resistivity. Furthermore, due to the generation of Zn boundaries along the SnO_2/ZnO heterointerfaces, a new energy band configuration will be established (Figure 7). Because the sensor current will mainly flow through the SnO_2 grains, the SnO_2/Zn heterointerfaces should be considered. The presence of metallic Zn will donate a large amount of electrons to the neighboring SnO_2 grains, significantly reducing the resistivity. In Figure 7, due to the significant initial flow of electrons to the SnO_2 side from metallic Zn, the depletion of SnO_2 sides will be reduced, resulting in the downward band bending of conduction band level of SnO_2. Accordingly, the energy difference between the Fermi level and conduction band in the SnO_2-side of the grain boundaries will be significantly reduced. Through the removal of H_2, the change of metallic Zn to semiconducting ZnO will restore the original band configuration. This phenomenon corresponds to the significant additional modulation of resistance by the Zn metallization effect.

Figure 5 indicates that the sensor response decreases as the grain size increases. In order to explain this observation, we presented Figure 8, which shows the change of grain/grain

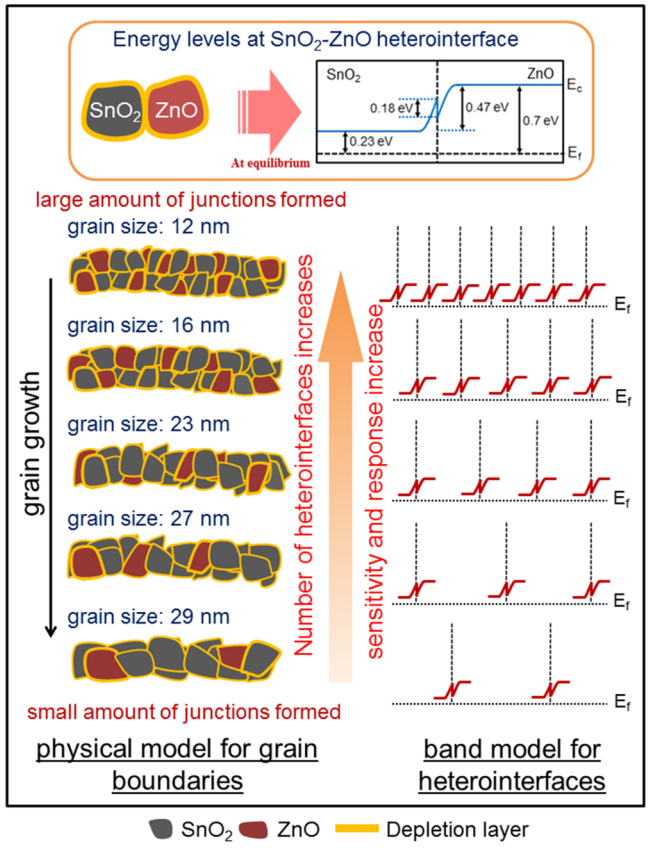

Figure 8. Schematic illustration of the effect of grain size on the amount of junction interfaces.

DOI: 10.1021/acsami.5b08416
ACS Appl. Mater. Interfaces 2016, 8, 2486−2494

boundary morphology by varying the grain size in the SnO_2-ZnO composite nanofibers. It clearly indicates that the number of grains and the amount of grain boundaries increase by decreasing the grain size in the range of 12−29 nm. Herein, we explain the grain size-dependence of H_2-sensor response by means of using the bifunctional mechanism. First, it is apparent that the amount of SnO_2-SnO_2 homointerfaces will increase by decreasing the SnO_2 grain size. With the nanofiber being mainly comprised of SnO_2 grains, the total amount of SnO_2-SnO_2 grain boundaries (i.e., homointerfaces) will increase by decreasing the grain size. As explained previously, the absorbed oxygen extracts electrons from the SnO_2, establishing the potential barriers. The potential barrier will be lowered by the reaction of introduced H_2 with surface oxygen. The change of the height of the potential barrier changes the electron flow, resulting in the modulation of resistance. Accordingly, the total modulation of resistance, which will be directly related to the sensor response, is proportional to the amount of SnO_2-SnO_2 grain boundaries (i.e., homointerfaces). In particular, the amount of homointerfaces is related to the total area of SnO_2-SnO_2 grain boundaries. Second, SnO_2-ZnO heterojunctions also contribute to the enhancement of sensing behavior. In particular, the SnO_2-ZnO heterojunctions provide the significant amount of modulation of resistance by the Zn metallization effect, playing a crucial role in sensing. Since the amount of ZnO nanograin is much smaller than that of SnO_2 grain, the ZnO nanograin will be usually surrounded by SnO_2 grains. Accordingly, if the grain size decreases (in this case, the sizes of both SnO_2 and ZnO grains will decrease), not only the number but also the total area of SnO_2-ZnO heterointerfaces will be increased (Figure 8). For a smaller grain-sized sensor, which can be fabricated with a shorter calcination time, the total amount of heterojunctions and homojunctions will be larger, resulting in a stronger sensor response. On the other hand, in the case of a larger grain-sized sensor, the total amount of heterojunctions and homojunctions will be smaller, resulting in a weaker sensor response. The initial resistances of the SnO_2-ZnO composite nanofiber sensors with various grain sizes are plotted in Figure S3. The nanofibers with larger grain sizes exhibited a lower initial resistance due to a reduction in the total amount of SnO_2-SnO_2 and SnO_2-ZnO junctions. Because the SnO_2-ZnO heteorjunctions are supposed to play a key role in enhancing the H_2 sensitivity, it is important to understand that the total amount (i.e., area and number) of SnO_2-ZnO heteorjunctions increases by decreasing the grain size (Figure 8).

To investigate the selective H_2-sensing capabilities of the SnO_2-ZnO composite nanofiber sensors, we analyzed the responses to other gases. Figure 9 shows the sensor responses at a concentration of 0.1 ppm. The sensor responses to H_2, C_2H_5OH, C_6H_6, CO, C_7H_8, NO_2, SO_2, H_2S, and CO_2 gases were 78.0, 29.9, 19.7, 12.2, 9.7, 3.3, 3.2, 2.6, and 2.5, respectively, revealing that the composite nanofibers are particularly sensitive to H_2 gas. However, the sensor response to other gases is still rather high even at a low concentration of 0.1 ppm. The differences in sensor response are mainly due to the different sensing mechanisms of other gases. For example, ethanol gas molecules are involved in a variety of reactions including decomposition or oxidation due to the acid−base properties of SnO_2 and ZnO.[32,33] Therefore, we surmise that the above-mentioned hydrogen-induced metallization phenomenon contributes to the enhancement of sensing capability with respect to H_2 gas.

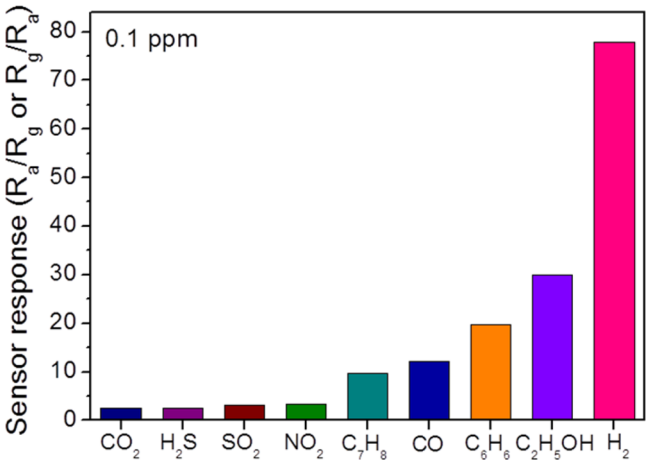

Figure 9. Summary of sensor responses of the sensors fabricated with SnO_2-ZnO composite nanofibers to 0.1 ppm of H_2, C_2H_5OH, C_6H_6, CO, C_7H_8, NO_2, SO_2, H_2S, and CO_2.

First, we investigated the stability of the $0.90SnO_2$-$0.10ZnO$ nanofibers in humid environment. In Figure 10, we compared

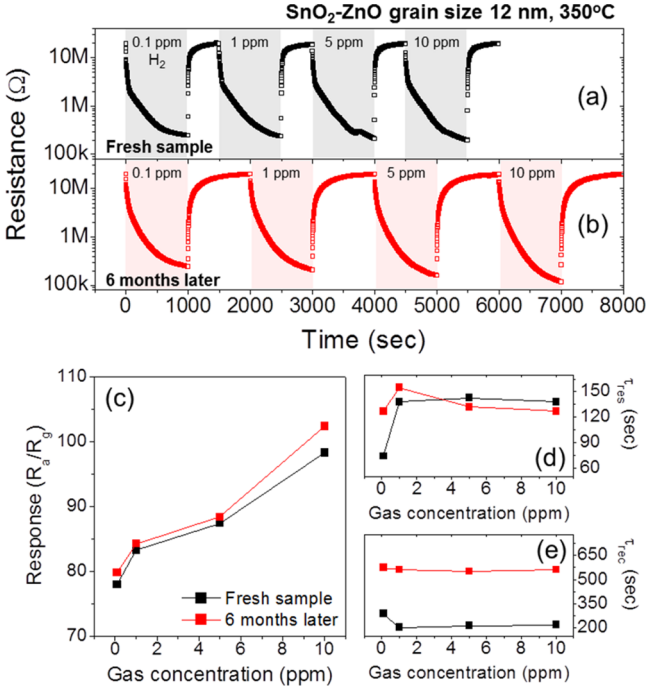

Figure 10. Stability of the SnO_2-ZnO composite nanofibers in humid environment (RH 60% @ 25 °C) for 6 months. Dynamic resistance curves of (a) the original sensors and (b) the sensors that were preserved in the humid environment for 6 months. (c−e) Comparison of (c) the sensing responses, (d) response times, and (e) recovery times of the sensors that were preserved in the humid environment for 6 months compared with that of the original sensor.

the sensing response curve of the sensor, which was preserved in the humid environment (RH 60% @ 25 °C) for 6 months, with that of the original sensor. After 6 months, the sensor responses to H_2 gas at 0.1, 1, 5, and 10 ppm were changed from 78.0, 83.2, 87.4, and 98.3 to 79.8, 84.2, 88.4, and 102.3, respectively, (i.e., increased by 2.3, 1.2, 1.1, and 4.1%), revealing no change in the error range (±5%) (Table S2). After 6 months, the response times at 0.1, 1, 5, and 10 ppm were

DOI: 10.1021/acsami.5b08416
ACS Appl. Mater. Interfaces 2016, 8, 2486−2494

changed from 74, 138, 143, and 138 s to 127, 155, 132, and 127 s, respectively, (i.e., increased by 71.6, 12.3, −7.7, and −8.0%) (Table S3). After 6 months, the recovery times at 0.1, 1, 5, and 10 ppm were changed from 289, 205, 215, and 221 s to 574, 561, 553, and 562 s, respectively (i.e., increased by 98.6, 173.7, 157.2, and 154.3%) (Table S3). In particular, recovery times were significantly increased by keeping the sample in the humid environment. It is possible that the water adsorption in the humid environment will degrade the sensing capabilities, resulting in the longer recovery time.

Second, we investigated the effect of humidity in sensing test on the sensing behaviors of the $0.90SnO_2$-0.10ZnO nanofibers. Figure 11 compares the response curves of the $0.90SnO_2$-0.10ZnO nanofibers in humid air (RH 30% @ 350 °C) with those in dry air (RH 0% @ 350 °C). The sensor responses of the $0.90SnO_2$-0.10ZnO nanofibers sensors to H_2 gas at concentrations of 0.1, 1, 5, and 10 ppm, in humid air are 19.5, 35.6, 49.7, and 69.9, respectively (Table S4). The sensor responses of the $0.90SnO_2$-0.10ZnO nanofibers sensors to H_2 gas at concentrations of 0.1, 1, 5, and 10 ppm, in humid air are decreased by 75.0, 57.2, 43.1, and 28.9%, in comparison to those in dry air, respectively. Also, the response times in humid air are increased by 112.2, 123.9, 214.0, and 407.2%, in comparison to those in dry air, at H_2 gas at concentrations of 0.1, 1, 5, and 10 ppm, respectively (Table S5). Also, the recovery times in humid air are increased by 17.3, 68.3, 25.1, and 28.5%, in comparison to those in dry air, at H_2 gas at concentrations of 0.1 1, 5, and 10 ppm, respectively (Table S5).

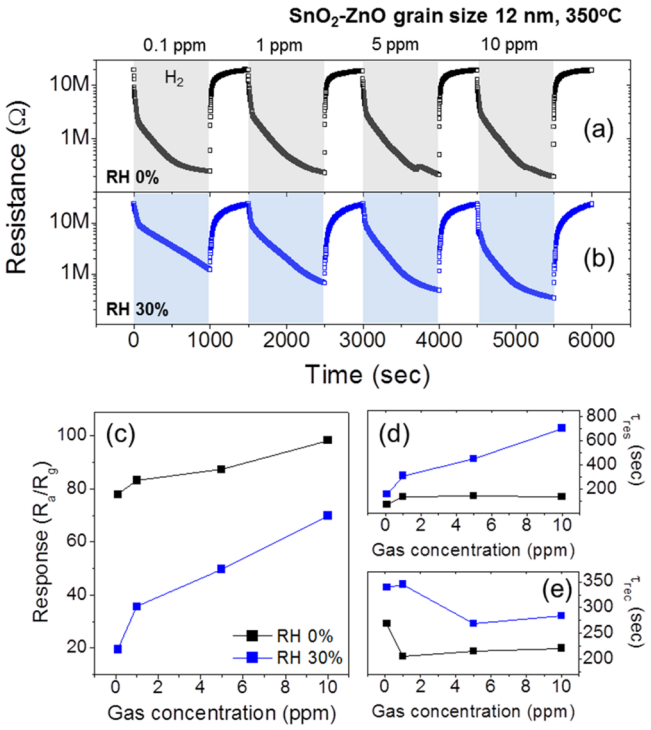

Figure 11. Effect of humidity in sensing test on the sensing behaviors of the SnO_2-ZnO composite nanofibers. The H_2 concentrations were set to 0.1, 1, 5, and 10 ppm. (a, b) Comparison of dynamic resistance curves of the SnO_2-ZnO composite nanofibers (b) in humid air (RH 30%) with those (a) in dry air (RH 0%). Comparison of (c) sensor responses, (d) response times, and (e) recovery times of the SnO_2-ZnO composite nanofibers in humid air (RH 30%) with those in dry air (RH 0%).

It is possible that the water adsorption in the humid environment will lower the sensitivity (i.e., sensor response) of the sensors. The reaction between the surface oxygen and the water molecules results in a decrease in baseline resistance of the gas sensor and thus decreases the sensitivity.[34] Also, the adsorption of water molecules leads to less chemisorption of oxygen species and/or H_2 gas molecules on the SnO_2 surface because of the decrease in the adsorption area that is responsible for the sensor response. Accordingly, the incoming H_2 gas has difficulty in donating sufficient amount of electrons to nanofibers. Therefore, it will take a longer time to attain the highest value of the given sensor response values, resulting in a longer response time.

Up to the present, there have been a variety of works, which are related to the ZnO-SnO_2 composite sensors. Some of them proposed the mechanisms, in which the ZnO-SnO_2 composites enhanced the sensing capabilities. Liangyuan et al. indicated that the enhanced NO_2 sensing of the ZnO-SnO_2 nanocomposites was related to the chemical interactions which involved the adsorption of gases and reaction with O_2 and also to changes in electronic bind energies in the composites.[35] Also, Park et al. proposed that a highly sensitive NO_2 response of the SnO_2-ZnO hybrid nanofiber-based sensor is associated with the extra adsorption due to nanocrystalline SnO_2 coating and the charge transfer occurring between SnO_2 and ZnO.[36] In the SnO_2-ZnO thin film sensor, the higher rate of adsorption and oxidation of ethanol at the heterostructure containing two centers with different reductive-oxidative and acid−base properties was suggested as one probable reasons for the successful discrimination between ethanol and acetone.[33] In the SnO_2-ZnO thick film gas sensors, the huge improvement in the response and selectivity of the sensors to ethanol by ZnO doping is possibly due to the presence of Zn^{2+} species in SnO_2 that create a heterostructure containing two centers with different reductive-oxidative and acid−base properties that facilitate electronic interactions.[37] Several research groups suggest that the presence of ZnO-SnO_2 heterojunctions brings about the surface depletion layer and the potential barrier built in the junctions, in case of core−shell nanofibers,[18] core−shell nanowires,[38] SnO_2/ZnO hierarchical nanostructures,[39] hollow hierarchical SnO_2-ZnO composite nanofibers,[40] and ZnO-SnO_2-based composite films.[41] Huang et al. postulated that the abnormal sensing behavior, exhibiting concentration-dependent n-p-n transitions for its sensing response to H_2 gas, can be explained by the formation of n-ZnO/p-Zn-O-Sn/n-SnO_2 heterojunction structures, by means of ZnO surface modification to SnO_2 nanorod sensor.[42] In order to explain the sensing mechanisms in more detail, Mondal et al. and Tang et al. presented the energy band diagrams in regard to the SnO_2-ZnO heterojunctions.[41,42] Apart from the ZnO-SnO_2 composites, Liewhiran et al. studied the flame-spray-made SnO_2 nanoparticles for toxic and flammable gas-sensing applications[43] and subsequently attained the high response of $\sim 1 \times 10^4$ by using the Pd-loaded SnO_2 films films.[44] Also, Samerjain et al. reported the high response of 1.34×10^5 with Pt-loaded WO_3 films.[45] By the way, the above sensing tests were carried out at H_2 concentrations ranging from 0.01 to 1 vol % in dry air.

Furthermore, very recently, in explaining the prominent sensing behavior of the SnO_2-ZnO composite nanofibers to H_2 gas at concentrations in the range of 0.1−10 ppm, we proposed the bifunctional mechanism of SnO_2 homointerfaces and SnO_2-ZnO heterojunctions. In particular, we indicated that the metallization effect between ZnO and SnO_2 nanograins played

DOI: 10.1021/acsami.5b08416
ACS Appl. Mater. Interfaces 2016, 8, 2486−2494

an important role in enhancing the H_2-sensing behavior.[15] In the present work, we also utilized the metallization effect to explain the enhanced the H_2-sensing behavior. Also, we presented the energy band diagrams, which are comprised of SnO_2 and ZnO nanograins. However, in the present work, in contrast to the previous ones, we explained the associated sensing mechanisms in a more scientific and realistic way. We considered a new energy band configuration with the SnO_2/Zn heterointerfaces, due to the generation of Zn boundaries along the SnO_2/ZnO heterointerfaces, successfully explaining the significant additional modulation of resistance by the Zn metallization effect. Furthermore, in order to explain this observation, in which the sensor response decreases as the grain size increases, we presented the schematic diagrams, exhibiting the change in grain/grain boundary morphology by varying the grain size in the SnO_2-ZnO composite nanofibers.

4. CONCLUSIONS

We investigated the effect of grain size on the sensing capability of SnO_2-ZnO composite nanofibers fabricated through an electrospinning technique. The growth of nanograins in the composite nanofibers was accomplished under isothermal conditions. The nanofibers were comprised of a mixture of ZnO and SnO_2 grains. The H_2 sensing characteristics of the sensors fabricated from the ZnO-SnO_2 composite nanofibers with different grain sizes were examined at 350 °C with H_2 concentrations in the range of 0.1−10 ppm. The sensor with the smallest nanograins (i.e., 12 nm) showed the best sensing properties. In addition, the SnO_2-ZnO composite nanofibers exhibited better sensing behavior for H_2 gas compared to other gases including ethanol, benzene, toluene, and CO. The selective improvement in sensing behavior to H_2 gas compared to other gases will be mainly ascribed to the SnO_2-ZnO heterointerfaces, which will be enhanced by decreasing the grain size. The excellent sensing performance of the SnO_2-ZnO composite nanofiber sensors to H_2 is a result of the bifunctional sensing mechanism. The existence of a larger amount of SnO_2-ZnO heterojunctions as well as SnO_2-SnO_2 homojunctions in cases of smaller grain size is likely to contribute to the higher response of composite nanofibers. In particular, H_2-induced metallization in grain boundaries of SnO_2-ZnO heterointerfaces will significantly enhance the H_2-sensing abilities.

■ ASSOCIATED CONTENT

Supporting Information

The Supporting Information is available free of charge on the ACS Publications website at DOI: 10.1021/acsami.5b08416.

Figure showing the variation in initial resistance of SnO_2-ZnO composite nanofiber sensors with various grain sizes (PDF)

■ AUTHOR INFORMATION

Corresponding Authors

*E-mail: hyounwoo@hanyang.ac.kr.

*E-mail: sangsub@inha.ac.kr.

Author Contributions

H.W.K. and S.S.K. conceived the study, designed the experiments, and prepared the manuscript. A.K. and Z.U.A. performed the experiments. All authors approved the final version of the paper.

Notes

The authors declare no competing financial interest.

■ ACKNOWLEDGMENTS

This work was supported by a National Research Foundation of Korea (NRF) grant funded by the Korean government (MEST) (NRF-2013R1A2A2A01068438).

■ REFERENCES

(1) Buttner, W. J.; Post, M. B.; Burgess, R.; Rivkin, C. An Overview of Hydrogen Safety Sensors and Requirements. *Int. J. Hydrogen Energy* **2011**, *36*, 2462−2470.

(2) Hübert, T.; Boon-Brett, L.; Palmisano, V.; Bader, M. A. Developments in Gas Sensor Technology for Hydrogen Safety. *Int. J. Hydrogen Energy* **2014**, *39*, 20474−20483.

(3) Hsu, C.-S.; Chen, H.-I.; Chou, P.-C.; Liou, J.-K.; Chen, C.-C.; Chang, C.-F.; Liu, W.-C. Hydrogen-Sensing Properties of a Pd/AlGaN/GaN-Based Field-Effect Transistor under a Nitrogen Ambience. *IEEE Sens. J.* **2013**, *13*, 1787−1793.

(4) Hübert, T.; Boon-Brett, L.; Black, G.; Banach, U. Hydrogen Sensors-A Review. *Sens. Actuators, B* **2011**, *157*, 329−352.

(5) Lim, W.; Wright, J. S.; Gila, B. P.; Johnson, J. L.; Ural, A.; Anderson, T.; Ren, F.; Pearson, S. J. Room Temperature Hydrogen Detection Using Pd-Coated GaN Nanowires. *Appl. Phys. Lett.* **2008**, *93*, 072109−072112.

(6) Schedin, F.; Geim, A. K.; Morozov, S. V.; Hill, E. W.; Blake, P.; Katsnelson, M. I.; Novoselov, K. S. Detection of Individual Gas Molecules Adsorbed on Graphene. *Nat. Mater.* **2007**, *6*, 652−655.

(7) Liao, L.; Lu, H. B.; Li, J. C.; Liu, C.; Fu, D. J.; Liu, Y. L. The Sensitivity of Gas Sensor Based on Single ZnO Nanowire Modulated by Helium Ion Radiation. *Appl. Phys. Lett.* **2007**, *91*, 173110−173113.

(8) Katoch, A.; Choi, S.-W.; Kim, H. W.; Kim, S. S. Highly Sensitive and Selective H_2 Sensing by ZnO Nanofibers and the Underlying Sensing Mechanism. *J. Hazard. Mater.* **2015**, *286*, 229−235.

(9) Katoch, A.; Choi, S.-W.; Sun, G.-J.; Kim, S. S. An Approach to Detecting a Reducing Gas by Radial Modulation of Electron-Depleted Shells in Core−Shell Nanofibers. *J. Mater. Chem. A* **2013**, *1*, 13588−13596.

(10) Xiong, K.; Robertson, J.; Clark, S. J. Behavior of Hydrogen in Wide Band Gap Oxides. *J. Appl. Phys.* **2007**, *102*, 083710−083723.

(11) Park, J. Y.; Asokan, K.; Choi, S.-W.; Kim, S. S. Growth Kinetics of Nanograins in SnO_2 Fibers and Size Dependent Sensing Properties. *Sens. Actuators, B* **2011**, *152*, 254−260.

(12) Viter, R.; Katoch, A.; Kim, S. S. Grain Size Dependent Bandgap Shift of SnO_2 Nanofibers. *Met. Mater. Int.* **2014**, *20*, 163−167.

(13) Park, J. Y.; Kim, S. S. Growth of Nanograins in Electrospun ZnO Nanofibers. *J. Am. Ceram. Soc.* **2009**, *92*, 1691−1694.

(14) Asokan, K.; Park, J. Y.; Choi, S.-W.; Kim, S. S. Nanocomposite ZnO−SnO_2 Nanofibers Synthesized by Electrospinning Method. *Nanoscale Res. Lett.* **2010**, *5*, 747−752.

(15) Katoch, A.; Kim, J.-H.; Kwon, Y. J.; Kim, H. W.; Kim, S. S. Bifunctional Sensing Mechanism of SnO_2-ZnO Composite Nanofibers for Drastically Enhancing the Sensing Behavior in H_2 Gas . *ACS Appl. Mater. Interfaces* **2015**, *7*, 11351−11358.

(16) Choi, S.-W.; Park, J. Y.; Kim, S. S. Dependence of Gas Sensing Properties in ZnO Nanofibers on Size and Crystallinity of Nanograins. *J. Mater. Res.* **2011**, *26*, 1662−1665.

(17) Kim, H. W.; Shim, S. H.; Lee, J. W.; Park, J. Y.; Kim, S. S. $Bi_2Sn_2O_7$ Nanoparticles Attached to SnO_2 Nanowires and Used as Catalysts. *Chem. Phys. Lett.* **2008**, *456*, 193−197.

(18) Choi, S.-W.; Park, J. Y.; Kim, S. S. Synthesis of SnO_2-ZnO Core-Shell Nanofibers Via a Novel Two-Step Process and Their Gas Sensing Properties. *Nanotechnology* **2009**, *20*, 465603−465609.

(19) Park, J. Y.; Choi, S. W.; Lee, J. W.; Lee, C.; Kim, S. S. Synthesis and Gas Sensing Properties of TiO_2-ZnO Core-Shell Nanofibers. *J. Am. Ceram. Soc.* **2009**, *92*, 2551−2554.

(20) Choi, S.-W.; Katoch, A.; Zhang, J.; Kim, S. S. Electrospun Nanofibers of CuO-SnO_2 Nanocomposite as Semiconductor Gas Sensors for H_2S Detection. *Sens. Actuators, B* **2013**, *176*, 585−591.

DOI: 10.1021/acsami.5b08416
ACS Appl. Mater. Interfaces 2016, 8, 2486−2494

(21) Choi, S.-W.; Park, J. Y.; Kim, S. S. Growth Behavior and Sensing Properties of Nanograins in CuO Nanofibers. *Chem. Eng. J.* **2011**, *172*, 550−556.
(22) Lee, D. S.; Lee, J. H.; Lee, Y. H.; Lee, D. D. GaN Thin Films as Gas Sensors. *Sens. Actuators, B* **2003**, *89*, 305−310.
(23) Al-Hardan, N. H.; Abdullah, M. J.; Abdul Aziz, A. Sensing Mechanism of Hydrogen Gas Sensor Based on RF-Sputtered ZnO Thin Films. *Int. J. Hydrogen Energy* **2010**, *35*, 4428−4434.
(24) Park, J. Y.; Choi, S.-W.; Kim, S. S. A Model for The Enhancement of Gas Sensing Properties in SnO_2-ZnO Core-Shell Nanofibers. *J. Phys. D: Appl. Phys.* **2011**, *44*, 205403−205407.
(25) Neri, G.; Bonavita, A.; Micali, G.; Rizzo, G.; Pinna, N.; Niederberger, M. In_2O_3 and Pt-In_2O_3 Nanopowders for Low Temperature Oxygen Sensors. *Sens. Actuators, B* **2007**, *127*, 455−462.
(26) Wang, C.; Zhou, G.; Li, J.; Yan, B.; Duan, W. Hydrogen-Induced Metallization of Zinc Oxide ($2\bar{1}\bar{1}0$) Surface and Nanowires: The Effect of Curvature. *Phys. Rev. B: Condens. Matter Mater. Phys.* **2008**, *77*, 245303−245310.
(27) Xu, H.; Fan, W.; Rosa, A. L.; Zhang, R. Q.; Frauenheim, Th. Hydrogen and Oxygen Adsorption on ZnO Nanowires: A First-Principles Study. *Phys. Rev. B: Condens. Matter Mater. Phys.* **2009**, *79*, 073402−073406.
(28) Wagner, C. D.; Riggs, W. M.; Davis, L. E.; Moulder, J. F.; Muilenberg, G. E. *Handbook of X-Ray Photoelectron Spectroscopy*; Perkin-Elmer: Eden Prairie, MN, 1979.
(29) *NIST X-ray Photoelectron Spectroscopy Database*; National Institute of Standards and Technology: Gaithersburg, TN; http://srdata.nist.gov/xps/.
(30) Moulder, J. F.; Stickle, W. F.; Sobol, P. E.; Bomben, K. D. *Handbook of X-ray Photoelectron Spectroscopy*; Chastain, J., Ed.; Perkin-Elmer: New York, 1992.
(31) Islam, M. N.; Ghosh, T. B.; Chopra, K. L.; Acharya, H. N. XPS and X-ray diffraction studies of aluminum-doped zinc oxide transparent conducting films. *Thin Solid Films* **1996**, *280*, 20−25.
(32) Jinkawa, T.; Sakai, G.; Tamaki, J.; Miura, N.; Yamazoe, N. Relationship Between Ethanol Gas Sensitivity and Surface Catalytic Property of Tin Oxide Sensors Modified with Acidic or Basic Oxides. *J. Mol. Catal. A: Chem.* **2000**, *155*, 193−200.
(33) Kim, K.-W.; Cho, P.-S.; Kim, S.-J.; Lee, J.-H.; Kang, C.-Y.; Kim, J.-S.; Yoon, S.-J. The Selective Detection of C_2H_5OH Using SnO_2-ZnO Thin Film Gas Sensors Prepared by Combinatorial Solution Deposition. *Sens. Actuators, B* **2007**, *123*, 318−324.
(34) Gong, J.; Chen, Q.; Lian, M.-R.; Liu, N.-C.; Stevenson, R. G.; Adami, F. Micromachined Nanocrystalline Silver Doped SnO_2 H_2S Sensor. *Sens. Actuators, B* **2006**, *114*, 32−39.
(35) Liangyuan, C.; Shouli, B.; Guojun, Z.; Dianqing, L.; Aifan, C.; Liu, C. C. Synthesis of ZnO-SnO_2 Nanocomposites by Microemulsion and Sensing Properties for NO_2. *Sens. Actuators, B* **2008**, *134*, 360−366.
(36) Park, J.-A.; Moon, J.; Lee, S.-J.; Kim, S. H.; Chu, H. Y.; Zyung, T. SnO_2-ZnO Hybrid Nanofibers-Based Highly Sensitive Nitrogen Dioxides Sensor. *Sens. Actuators, B* **2010**, *145*, 592−595.
(37) Hemmati, S.; Firooz, A. A.; Khodadadi, A. A.; Mortazavi, Y. Nanostructured SnO_2-ZnO Sensors: Highly Sensitive and Selective to Ethanol. *Sens. Actuators, B* **2011**, *160*, 1298−1303.
(38) Hwang, I.-S.; Kim, S.-J.; Choi, J.-K.; Choi, J.; Ji, H.; Kim, G.-T.; Cao, G.; Lee, J.-H. Synthesis and Gas Sensing Characteristics of Highly Crystalline ZnO-SnO_2 Core-Shell Nanowires. *Sens. Actuators, B* **2010**, *148*, 595−600.
(39) Khoang, N. D.; Trung, D. D.; Van Duy, N.; Hoa, N. D.; Van Hieu, N. Design of SnO_2/ZnO Hierarchical Nanostructures for Enhanced Ethanol Gas-Sensing Performance. *Sens. Actuators, B* **2012**, *174*, 594−601.
(40) Tang, W.; Wang, J.; Yao, P.; Li, X. Hollow Hierarchical SnO_2-ZnO Composite Nanofibers with Heterostructure Based on Electrospinning Method for Detecting Methanol. *Sens. Actuators, B* **2014**, *192*, 543−549.
(41) Mondal, B.; Basumatari, B.; Das, J.; Roychaudhury, C.; Saha, H.; Mukherjee, N. ZnO-SnO_2 Based Composite Type Gas Sensor for Selective Hydrogen Sensing. *Sens. Actuators, B* **2014**, *194*, 389−396.
(42) Huang, H.; Gong, H.; Chow, C. L.; Guo, J.; White, T. J.; Tse, M. S.; Tan, O. K. Low-Temperature Growth of SnO_2 Nanorod Arrays and Tunable n-p-n Sensing Response of a ZnO/SnO_2 Heterojunctions for Exclusive Hydrogen Sensors. *Adv. Funct. Mater.* **2011**, *21*, 2680−2686.
(43) Liewhiran, C.; Tamaekong, N.; Wisitsoraat, A.; Phanichphant, S. Highly Selective Environmental Sensors Based on Flame-Spray-Made SnO_2 Nanoparticles. *Sens. Actuators, B* **2012**, *163*, 51−60.
(44) Liewhiran, C.; Tamaekong, N.; Wisitsoraat, A.; Tuantranont, A.; Phanichphant, S. Ultra-Sensitive H_2 Sensors Based on Flame-Spray-Made Pd-Loaded SnO_2 Sensing Films. *Sens. Actuators, B* **2013**, *176*, 893−905.
(45) Samerjai, T.; Tamaekong, N.; Liewhiran, C.; Wisitsoraat, A.; Tuantranont, A.; Phanichphant, S. Selectivity Towards H_2 Gas by Flame-Made Pt-Loaded WO_3 Sensing Films. *Sens. Actuators, B* **2011**, *157*, 290−297.

DOI: 10.1021/acsami.5b08416
ACS Appl. Mater. Interfaces 2016, 8, 2486−2494